Radio receivers based on spin-torque diodes as energy detectors

Imadeddine Bendjeddou, Ahmed Sidi El Valli, Artem Litvinenko, Yannis Le Guennec, Florence Podevin, Romain Lebrun, Sylvain Bourdel, Emmanuel Pistono, Dominique Morche, Alex Jenkins, et al.

Electrical Modeling of Spin-Torque Diodes used as Radiofrequency Detectors: a Step-by-Step Methodology for Parameter Extraction

I. Bendjeddou[1][2][3], *Student Member, IEEE*, M. Jotta Garcia[4], A. Sidi El Valli[5], V. Cros[4], U. Ebels[5], A. Jenkins[6], R. Ferreira[6], R. Dutra[6], D. Morche[1], E. Pistono[2], S. Bourdel[2], *Member, IEEE*, Y. Le Guennec[3] and F. Podevin[2], *Member, IEEE*

[1] LETI, CEA, Minatec Campus, Grenoble 38054, FR

[2] Univ. Grenoble Alpes, CNRS, Grenoble INP, TIMA, Grenoble 38031, FR

[3] Univ. Grenoble Alpes, CNRS, Grenoble INP, GIPSA-Lab, Saint-Martin-d'Hères 38400, FR

[4] Unité Mixte de Physique, CNRS, Thales, Université Paris-Saclay, Palaiseau 91767, FR

[5] Univ. Grenoble Alpes, CEA, CNRS, Grenoble INP, SPINTEC, Grenoble 38054, FR

[6] International Iberian Nanotechnology Laboratory (INL), Braga, PRT

In this paper, we present an electrical model for nanoscale spintronic radiofrequency (RF) detectors called spin torque diodes (STD). A complete methodology for model parameter extraction is proposed. An equivalent electrical circuit for STD is derived and integrates a modeling of the device resistance non-linearity together with the spin-torque diode effect. A detailed step-by-step methodology is presented to extract the model parameters using conventional DC measurements, RF scattering parameters (S-parameters), continuous wave and power characterizations. After parameter extraction, a comparison with measurements of a single STD successfully validates the model. Finally, the proposed STD electrical model is used to anticipate the behavior of a 2-STD based RF detector architecture. Simulation results highlight the interest of the proposed modeling approach to investigate suitable RF detector architectures to enhance RF-to-DC conversion efficiency for single or multiband RF detection.

Index Terms—**Spin-torque diodes, radiofrequency detector, electrical modeling, parameter extraction, RF-to-DC conversion.**

I. Introduction

SPINTRONIC devices have raised a huge interest in the last decades, leading to remarkable breakthroughs in magnetic memories [1], neuromorphic circuits [2], [3], sensors [4], spin-torque nano-oscillators (STNOs) or nanoscale spin-torque diodes (STDs) used as RF detectors [5]–[7]. In the context of radiofrequency (RF) communications, inherent rectifying effect of STD can be efficiently used as RF-to-DC converter for RF envelope detectors [8]–[10]. Indeed, STD offers considerable interests for RF detection. On the first hand, it provides narrow-band filtering capability, which is of crucial importance for RF detector selectivity, but also for detector sensitivity since any unfiltered out-of-band RF signal may directly interfere with the in-band signal envelope detection [11], [12]. On the second hand, STD shows nano-sized footprint, which paves the way for integration of multiple STDs into a single RF detector chip with the objective of multiband RF detection or RF energy harvesting [9]. Constant efforts are being made in spintronic technology and circuit design to enhance STD energy efficiency and selectivity [13], [14], making them more and more competitive for practical applications in RF detection. However, the design of complex receiver based on multiple STD devices needs accurate electrical modeling especially to optimize both the sensitivity and the selectivity [15], [16]. Such an electrical model would highly facilitate the RF designer's task. Indeed, assembling multiple STD models into a complete RF detector architecture could address potential impedance matching issues, or problems associated to resonance frequency synchronization, leading to RF-to-DC conversion efficiency penalties when connecting multiple STD devices on a single chip [16], [17]. To make it easy to handle, an STD electrical model should be compact and model parameters should be easily extracted from conventional RF characterization measurements.

This article presents a compact electrical model for STD used as an RF continuous wave (CW) detector. To the authors' knowledge, this is the first time that such model is reported. This model integrates STD input and output impedance, STD rectifying and frequency selective spin-torque effects and RF power dependency of STD selectivity. This electrical model allows for an accurate prediction of RF-to-DC conversion efficiency in RF CW detection. To complete this approach, an exhaustive step-by-step methodology to extract model parameters from measurements is also described.

The rest of the article is organized as follows. Section II presents the STD electrical model. Section III develops an accurate methodology for the model parameter extraction from conventional RF measurements. Then, section IV illustrates a case study when a multiple STD-based RF detector architecture is considered. Conclusions and perspectives of this work are drawn in section V.

II. Electrical Model for STD

A. RF-to-DC conversion in STD

As a non-linear device, STD can be used as a rectifier circuit to achieve RF-to-DC conversion [9]. A simplified representation of a rectifier circuit is shown in Fig. 1. Basically, it is a non-linear resistance R_j, which is described by its non-linear $I(V)$ characteristics, V being delivered by an ideal voltage source. In STD, the input RF current can impact the magnetization dynamics of the device, which causes in return a change of the magneto-resistance with time. When

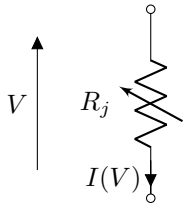

Fig. 1: Simplified electrical model for a rectifier circuit.

the RF frequency of the STD excitation signal corresponds to the natural resonance frequency of the STD, the RF current causes the resistance of the device - a magnetic tunnel junction (MTJ), to oscillate at the due to the magneto-resistance effect [18], [19]. The mixing of the resistance oscillation with the RF current originates a rectified current. This is the so-called "spin-torque diode effect" [20].

Taking into account both rectifying and resonance effects, the STD output current, I, can be expressed as a polynomial expansion of the RF excitation voltage, V, as:

$$I(V) = \frac{V}{R_0} + \gamma_{\text{rec}} \left[1 + G_{\text{spin}}(f_0)\right] V^2 + cV^3 + dV^4 + \ldots \quad (1)$$

where R_0 is the STD linear resistance, γ_{rec} (in A/V^2) is the rectifying coefficient, $G_{\text{spin}}(f_0)$ is the spin-torque gain which is dependent on the excitation frequency f_0, c (in A/V^3) and d (in A/V^4) are the third and fourth order non-linear coefficients, respectively. $G_{\text{spin}}(f_0)$ accounts for STD frequency selectivity as it acts as a band-pass filter for RF detection. Consequently, the non-linear junction resistance, $R_j = R_j(V)$ can be expressed as:

$$\frac{1}{R_j(V)} = \frac{1}{R_0} + \gamma_{\text{rec}} \left[1 + G_{\text{spin}}(f_0)\right] V + cV^2 + dV^3 + \ldots \quad (2)$$

Considering a continuous wave (CW) excitation, $V = V_{\text{RF}}(t) = V_{\text{RF}} \cos(2\pi f_0 t)$ and inserting this into (1), a DC current, I_{dc} is generated at the STD nodes. Note that only even order non-linear coefficients in (1) are responsible for DC current generation. Neglecting n-th high even order non-linear coefficients ($n \geq 4$) in (1), I_{dc} can be approximated as:

$$I_{\text{dc}} \approx \gamma_{\text{rec}} \frac{V_{\text{RF}}^2}{2} + G_{\text{spin}}(f_0) \gamma_{\text{rec}} \frac{V_{\text{RF}}^2}{2}. \quad (3)$$

The first term in (3) is the DC current issued from the STD rectifying effect, while, in the second term, the spin-torque gain, $G_{\text{spin}}(f_0)$ amplifies the generated rectified current when the excitation frequency, f_0, is close to the STD resonance frequency.

B. STD under Test

The devices under test are vortex based magnetic tunneling junctions characterized by a multi-layer structure consisting of two ferromagnetic layers blocks: a Synthetic Anti-Ferromagnet (SAF) and a free layer separated by a 1-nm thick MgO insulating layer. The free layer is constituted of 7 nm of NiFe and 2 nm of $CoFe_{40}B_{20}$, while the SAF is constituted of 2.6 nm of CoFe, formatting on top of an IrMn layer, separated by 0.7-nm of Ru from a second 2.6-nm thick CoFeB, leading to AF coupling between them. After lithography and etching steps, the junctions present a diameter D ranging from 440 to 450 nm (depending on the local etching). The tunneling magneto-resistance (TMR) is comprised between 70 and 100% while the resistance-area product is about 2 $\Omega \cdot \mu^2$. Neither external magnetic field nor external bias current are applied on the STD [21]. Fig. 2 shows the multilayer STD connected to Al electrodes and integrated into a Al_2O_2 substrate deposited on top of a Si wafer.

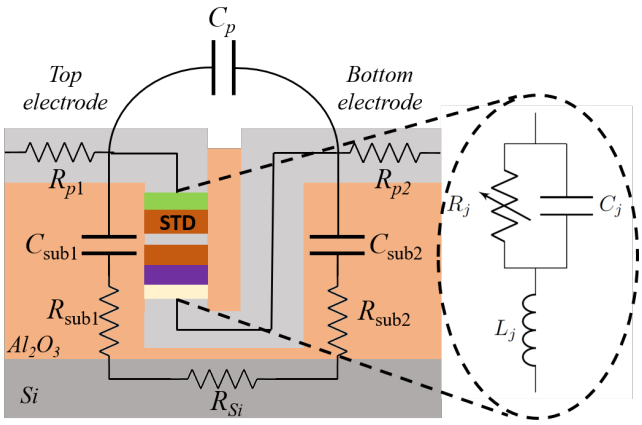

Fig. 2: Integrated STD device and related equivalent electrical elements.

The equivalent electrical elements of the integrated STD device together with surrounding electrical parasitic components from electrodes and substrates are reported in Fig. 2. R_j is the STD non-linear junction resistance, C_j and L_j are the STD junction capacitance and inductance, respectively. R_{p1} and R_{p2} represent the series resistances of the metallic pads (i.e. electrodes) and feeding lines. C_p represents the direct coupling capacitor from pad to pad. C_{sub1} and C_{sub2} represent the indirect coupling capacitors from pad to pad through the substrate, while R_{sub1}, R_{sub2} and R_{Si} represent the indirect coupling resistances from pad to pad through Al_2O_3 and Si substrates, respectively.

C. Compact electrical model for STD

The proposed electrical model for STD-based RF-to-DC converter is shown in Fig. 3 together with an input CW RF source at frequency f_0, with internal real impedance Z_{RF}. The non-linear resistance, R_j, is directly modeled by equ. (2) which integrates the non-linear rectifying effect and the frequency dependent spin-torque effect through $G_{\text{spin}}(f_0)$ (2). In Fig. 3, C_{sub} and R_{sub} represent the overall indirect coupling capacitor and resistance between pads and substrate, respectively. Referring to Fig. 2, $R_{\text{sub}} = R_{\text{sub1}} + R_{\text{sub2}} + R_{\text{Si}}$, and C_{sub} corresponds to the equivalent capacitance from C_{sub1} and C_{sub2} placed in series. R_p in Fig. 3 corresponds to the equivalent pad (i.e. electrode) resistor, $R_p = R_{p1} + R_{p2}$ in Fig. 2.

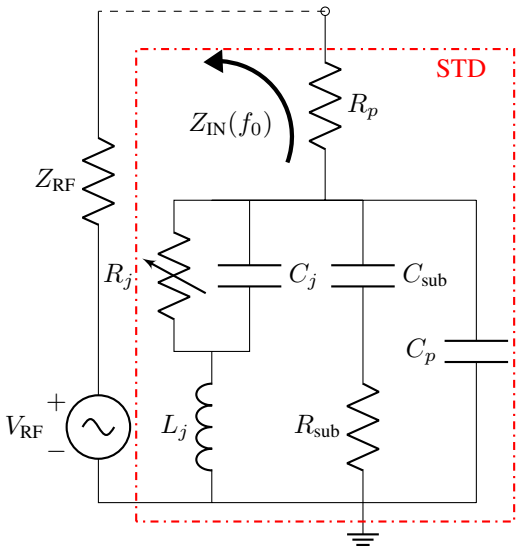

Fig. 3: Equivalent electrical model for STD connected to an RF source.

D. Effect of Impedance Mismatch

The STD complex input impedance, $Z_{\text{IN}}(f_0)$, is the frequency dependent input impedance of the STD equivalent circuit shown in Fig. 3. In most of the cases, impedance matching is not satisfied between the RF source real impedance, Z_{RF} and the STD input impedance, $Z_{\text{IN}}(f_0)$. As a consequence, impedance mismatch leads to a reflection coefficient, $\Gamma(f_0)$ which is defined as:

$$\Gamma(f_0) = \frac{Z_{\text{IN}}(f_0) - Z_{\text{RF}}}{Z_{\text{IN}}(f_0) + Z_{\text{RF}}}. \tag{4}$$

In the general case of impedance mismatch between the RF source and the STD input, I_{dc} (3) becomes:

$$I_{\text{dc}} \approx \gamma_{\text{rec}} \left[1 + G_{\text{spin}}(f_0)\right] |1 - \Gamma(f_0)^2)| \frac{|Z_{\text{IN}}(f_0)|}{4Z_{\text{RF}}} \frac{V_{\text{RF}}^2}{2}. \tag{5}$$

From equation (5), it can be seen that impedance mismatch directly impacts the RF-to-DC conversion efficiency. As a consequence, the STD equivalent electrical model should integrate impedance modeling together with non-linear $I(V)$ characteristics to accurately predict the RF-to-DC conversion efficiency [15].

III. Methodology for Model Parameter Extraction

This section presents a complete methodology to extract the STD model parameters from conventional DC and RF characterizations including scattering parameters (i.e. S-Parameters), continuous wave (CW) and power measurements.

A. DC Characterization

In order to extract the non-linear coefficients of $I(V)$ (1), a DC characterization of the STD device is first performed. The DC characterization set-up is shown in Fig. 4. A DC voltage, V_{dc}, is generated from a power supply with internal impedance, Z_{dc} and fed into the STD whilst a high precision ampere-meter is used to measure the generated DC current from the STD, $I_{\text{dc}}(V_{\text{dc}})$. Under DC voltage excitation, the STD electrical model shown in Fig. 3 is equivalent to the non-linear resistance, R_j, in series with R_p, leading to a STD input impedance $Z_{\text{IN}}(f = 0) = R_0 = R_j + R_p$. The measured $I_{\text{dc}}(V_{\text{dc}})$ characterization results are reported on Fig. 5 (red markers). As it can be seen on Fig. 5, $I_{\text{dc}}(V_{\text{dc}})$ is close to a linear function, i.e. the linear coefficient in $I_{\text{dc}}(V_{\text{dc}})$ is expected to be large when compared to the non-linear coefficients, γ_{rec} and c. Moreover, since the STD resonance frequency is a few hundreds of MHz (see section III.C), there is no spin-torque diode effect, i.e. $G_{\text{spin}}(f = 0) = 0$ in (1). A polynomial curve fitting (black plot in Fig. 5) is performed on the experimental

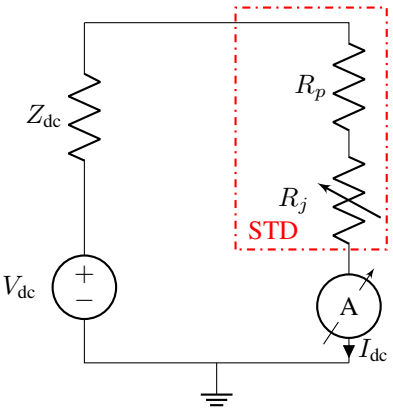

Fig. 4: DC characterization set-up for STD device.

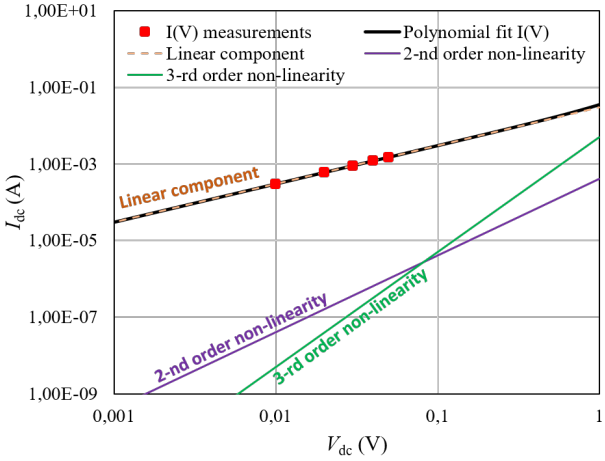

Fig. 5: Measured $I_{\text{dc}}(V_{\text{dc}})$ STD characteristics (red) and 3-rd order polynomial fit (black).

TABLE I: Extracted parameters from DC characterization

Parameter	Value
R_0 (Ω)	34.0
γ_{rec} (A/V^2)	0.0004
c (A/V^3)	0.0049

$I_{dc}(V_{dc})$ results in order to extract $1/R_0$, γ_{rec} and c parameters from (1). Linear component of $I_{dc}(V_{dc})$ in (1), i.e. V_{dc}/R_0, is reported in Fig. 5 as an orange dashed line. In Fig. 5, it can be seen that the polynomial extrapolation of $I_{dc}(V_{dc})$ slightly deviates from its linear component V_{dc}/R_0 when the 2-nd order non-linear term of $I_{dc}(V_{dc})$ (i.e. $\gamma_{rec}V_{dc}^2$ shown in purple color) and 3-rd order non-linear term (i.e. cV_{dc}^3 shown in green color) reach significant values while increasing V_{dc}. The extracted R_0, γ_{rec} and c parameter values are reported in Tab. I. The $I_{dc}(V_{dc})$ fitted values do not deviate more than 6.5% from the measurement results. Please note that R_0 determination also leads to the definition of the STD output impedance for $f = 0$, $Z_{OUT}(f = 0) = R_0$.

B. RF S-Parameter Characterization

STD reflection coefficient measurement has been performed with a R&S ZNB 9 kHz-8.5 GHz Vector Network Analyzer (VNA).

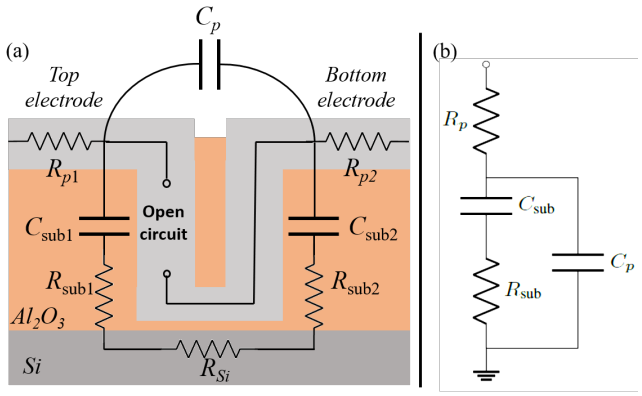

Fig. 6: Reference open circuit (a) and related equivalent circuit (b).

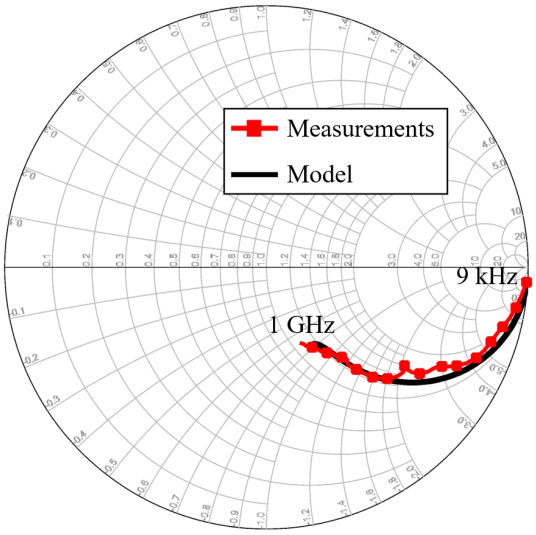

Fig. 7: Measured and simulated S_{11open} reflection coefficient for the reference open circuit in the frequency range [9 kHz - 1 GHz].

As a first step, we consider a so called "reference open circuit" which is identical to the one shown in Fig. 2 except that an open circuit is left instead of the STD junction, as shown in Fig. 6 (a), which leads to the equivalent circuit shown in Fig. 6 (b). The STD device top electrode is connected to the measurement port of the VNA while STD device bottom electrode is connected to the ground. Fig. 7 (red plot) reports the measured reflection coefficient $S_{11open} = \Gamma_{open}(f_0)$ for the reference open circuit, plotted in a Smith Chart for the frequency range [9 kHz, 1 GHz]. As expected, at low frequencies, the reference open circuit behaves as a perfect open load whilst, when increasing excitation frequency, the capacitive effect from C_{sub} and C_p is highlighted.

TABLE II: Extracted parameters from S_{11} characterization

Parameter	Quantity	Value
R_{sub} (Ω)	Substrate resistance	115
C_{sub} (pf)	Substrate capacitance	12
R_p (Ω)	Package resistance	1
C_p (pF)	Package capacitance	0.61
C_j (fF)	Junction capacitance	30
L_j (fH)	Junction inductance	50
$R_j(V)$ (Ω)	Junction resistance	see Tab. I

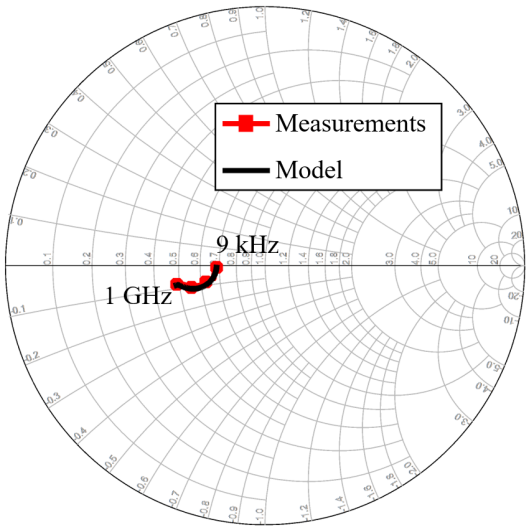

Fig. 8: Measured and simulated S_{11} reflection coefficient of the STD circuit in the frequency range [9 kHz - 1 GHz].

Then, the electrical model of Fig. 6 (b) is simulated using Keysight Advanced Design System (ADS) RF circuit design tool with its S-matrix solver. An optimization is performed to define R_p, C_p, R_{sub} and C_{sub} values so that the simulation results match the measurement results. The extracted values for R_p, C_p, R_{sub} and C_{sub} are reported in Tab. II and simulation results for S_{11open} are reported on Fig. 7 (black plot), showing very good agreement with the measurements. As a second step, the reflection coefficient of the STD device shown in Fig. 2 (i.e. including the STD) is determined. S_{11} measurement

result is shown on a Smith Chart in Fig. 8. By considering previously extracted parameter values for R_p, C_p, R_{sub} and C_{sub} (Tab. II) into the STD electrical model of Fig. 2, and the non-linear coefficients of $R_j(V)$ explicitly developed in equ. (2) and provided in Tab. I, C_j and L_j can be retrieved using the ADS optimization routine. The extracted values for C_j and L_j are reported in Tab. II whilst the simulation results for the STD device reflection coefficient are visible in Fig. 8 (black plot), showing a good agreement with measurements. At this step, the STD input impedance, $Z_{\text{IN}}(f_0)$ can be derived from the proposed electrical model for any RF excitation frequency in the range [9 kHz, 1 GHz] and STD output impedance at DC frequency is defined as $Z_{\text{OUT}}(f = 0) = R_0$.

C. RF CW Characterization

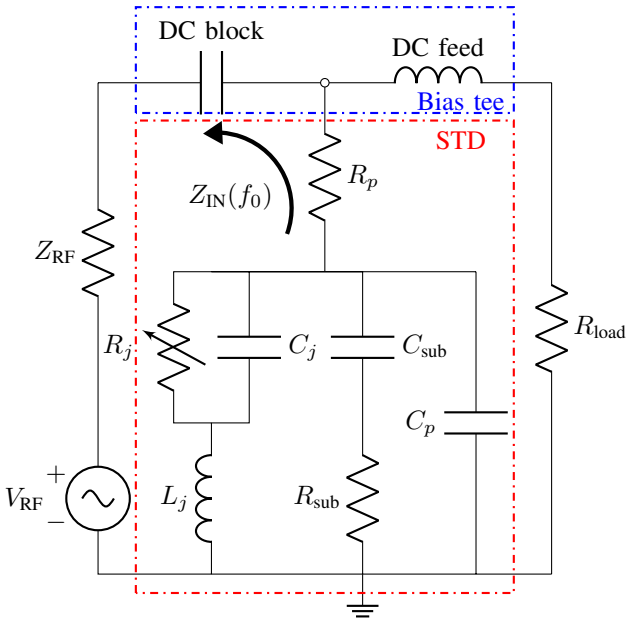

Fig. 9: CW characterization set-up connected to the STD equivalent electrical circuit.

The final step for STD model parameter extraction is to perform a CW characterization of the STD device. The set-up is shown in Fig. 9 where a CW excitation $V_{\text{RF}}(t) = V_{\text{RF}} \cos(2\pi f_0 t)$, from an RF source of internal impedance Z_{RF}, feeds the STD input. The power of the RF source is chosen equal to $P_{\text{RF}}(\text{dBm}) = 5$ dBm. For the load resistor, the STD device behaves as a DC voltage source of amplitude $R_0 I_{\text{dc}}$ and internal impedance $Z_{\text{OUT}}(f = 0) = R_0$. The STD output DC voltage, V_{dc}, is measured across the load resistor, R_{load}, with $R_{\text{load}} = 50\ \Omega$. A bias tee (see Fig. 9) is used to feed the STD device with the RF CW signal through a DC block capacitor, while I_{dc} is directed to the bias tee low frequency port through the DC feed inductor. Fig. 10 shows the measurement results (black plot) for V_{dc} as a function of the excitation frequency, f_0. V_{dc} reaches a maximum for an excitation frequency f_0 corresponding to the STD self-resonance frequency, $f_{\text{res}} \approx 150$ MHz for which the spin-torque gain effect is the highest.

Far from the STD resonance frequency, only rectifying effect occurs, i.e. $G_{\text{spin}}(f_0) = 0$ in (5), and an output

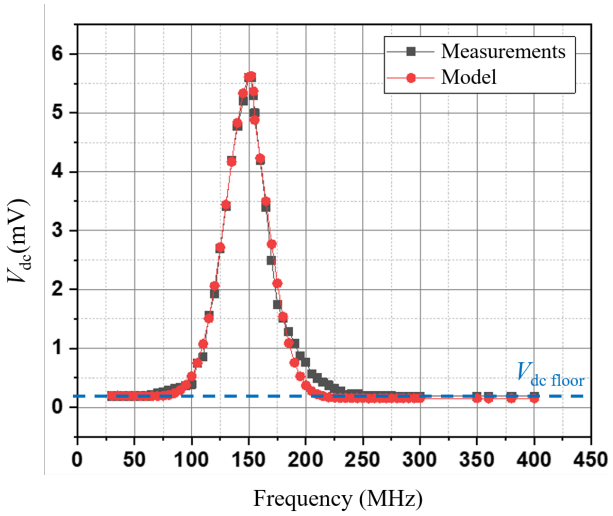

Fig. 10: Measured and simulated V_{dc} as a function of CW excitation frequency.

voltage floor, $V_{\text{dc floor}}$ (i.e. independent from f_0) is observed. Considering that the DC voltage on R_{load} is issued from a voltage divider bridge between the STD output impedance $Z_{\text{OUT}}(f = 0) = R_0$ and R_{load}, the voltage DC floor, $V_{\text{dc floor}}$ can be expressed as:

$$V_{\text{dc floor}} = \frac{R_0 R_{\text{load}}}{2(R_0 + R_{\text{load}})}(1 - |\Gamma(f = 0)|^2)\gamma_{\text{rec}} V_{\text{RF}}^2. \quad (6)$$

From the previous DC and S-parameters characterizations, we consider $R_0 = 34\ \Omega$, $|\Gamma(f = 0)|^2 = 0.036$ and $\gamma_{\text{rec}} = 0.0004\ \text{A/V}^2$. From (6), the theoretical value for $V_{\text{dc floor}}$ is evaluated at 0.125 mV, which is quite close to the experimental value of 0.150 mV visible in Fig. 10. The difference between theoretical and experimental $V_{\text{dc floor}}$ values may come from the power calibration of the RF source and/or the fact that higher order non-linear terms are neglected in $I(V)$ characteristics.

Close to the STD resonance frequency, spin-torque gain, $G_{\text{spin}}(f_0)$ is significant and the DC voltage on the load resistor, $V_{\text{dc}}(f_0)$ is expressed as:

$$V_{\text{dc}}(f_0) = \frac{R_0 R_{\text{load}}}{2(R_0 + R_{\text{load}})}(1 - |\Gamma(f_0)|^2)\gamma_{\text{rec}}\left[1 + G_{\text{spin}}(f_0)\right] V_{\text{RF}}^2. \quad (7)$$

From (6) and (7), on the basis that capacitive and inductive parasitics have low influence on the value of $|\Gamma(f_0)|^2$, meaning that $|\Gamma(f_0)|^2$ can be considered close to $|\Gamma(f = 0)|^2 = 0.036$, then $V_{\text{dc}}(f_0) \approx V_{\text{dc floor}}(1 + G_{\text{spin}}(f_0))$ and $G_{\text{spin}}(f_0)$ can be extracted. For our considered STD device, $G_{\text{spin}}(f_0)$ is approximated by a Gaussian function as:

$$G_{\text{spin}}(f_0) = G_{\text{res}} e^{-\frac{(f_0 - f_{\text{res}})^2}{2\sigma^2}}, \quad (8)$$

where G_{res} is the maximum spin-torque gain at the STD resonance frequency, f_{res} and σ^2 is the variance of $G_{\text{spin}}(f_0)$. Note that other fitting functions for describing $G_{\text{spin}}(f_0)$ could be employed in the proposed model, as, for example, the commonly used Lorentzian function [22]. We remind that

$G_{spin}(f_0)$ is responsible for the RF input band-pass filtering. For a Gaussian band-pass filter, the -3 dB band-pass bandwidth, $B_{\text{-3dB}}$ is related to the standard deviation, σ as:

$$B_{\text{-3dB}} = 2\sqrt{\ln 2}\sigma. \tag{9}$$

The STD electrical model shown in Fig. 3 is simulated using harmonic balance solver [23] from ADS simulation tool. In ADS software, a symbolically defined device (SDD) [24] is used to describe the non-linear junction resistance, $R_j(V)$ by entering the STD $I(V)$ characteristics (1), including $G_{spin}(f_0)$ extracted from (8). Parameters for the Gaussian function, $G_{spin}(f_0)$ are evaluated as $G_{res} = 1.39\ 10^6$ and $\sigma = 30$ MHz. Fig. 10 (red plot) shows the simulated output DC voltage, V_{dc} of the proposed STD model, as a function of the excitation frequency, f_0. From Fig. 10, it can be seen that the simulation results are in good accordance with measurement results.

D. RF Power Characterization

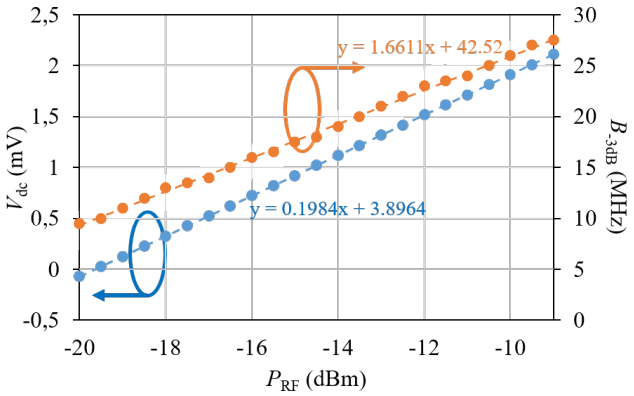

Fig. 11: Measured output DC voltage, V_{dc}, and -3dB bandwidth, $B_{\text{-3dB}}$, of the STD as a function on the input RF power in dBm, P_{RF}(dBm). Linear interpolations are represented with dashed lines.

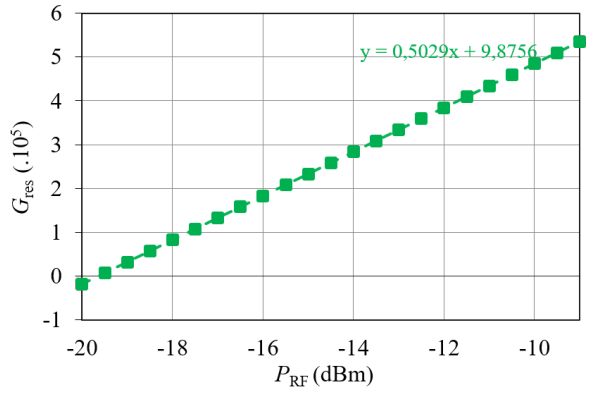

Fig. 12: Extracted G_{res} as a function of input RF power in dBm, P_{RF}(dBm). Linear interpolation is represented with dashed line.

Used as a RF-to-DC converter, the STD shows a dependency of G_{res} and $B_{\text{-3dB}}$ with respect to the input RF power. To take this dependency into account in the proposed electrical model, the STD output DC voltage at resonance frequency, $V_{dc}(f_{res})$ and STD bandwidth, $B_{\text{-3dB}}$ are measured as a function of the input RF power, P_{RF}. The measurement test bench is similar to the one shown in Fig. 9 except that the RF power is swept between -20 dBm and -9 dBm. Fig. 11 reports the measurement results for $V_{dc}(f_{res})$ and $B_{\text{-3dB}}$ as a function of P_{RF} (in dBm). A linear interpolation is realized to approximate $V_{dc}(f_{res})$ and $B_{\text{-3dB}}$ as a function of the RF input power, P_{RF} (in dBm) as:

$$\begin{aligned} V_{dc}(f_{res}) &= aP_{RF}(\text{dBm}) + b, \\ B_{\text{-3dB}} &= a'P_{RF}(\text{dBm}) + b', \end{aligned} \tag{10}$$

where P_{RF}(dBm) is the input RF power expressed in dBm and a, a', b and b' are linear interpolation parameters. After the linear interpolation process, it is found that $a = 0.0099$ V/dBm, $b = 0.1708$ V and $a' = 0.8305$ MHz/dBm, $b' = 8.4684$ MHz. Considering (7) with previously extracted parameters $R_0 = 34\ \Omega$, $\Gamma_0 = 0.036$, $\gamma_{rec} = 0.0004$ A/V^2 and $R_{load} = 50\ \Omega$, the dependency of G_{res} with P_{RF}(dBm) is obtained and represented in Fig. 12 where the related linear interpolation equation is reported. The linear equations describing $B_{\text{-3dB}}$ and G_{res} dependencies with P_{RF}(dBm) (equ. (10) and Fig. 12, respectively) are incorporated into (8) and finally into $I(V)$ characteristics (1) of the STD electrical model shown in Fig. 3.

E. Methodology Summary

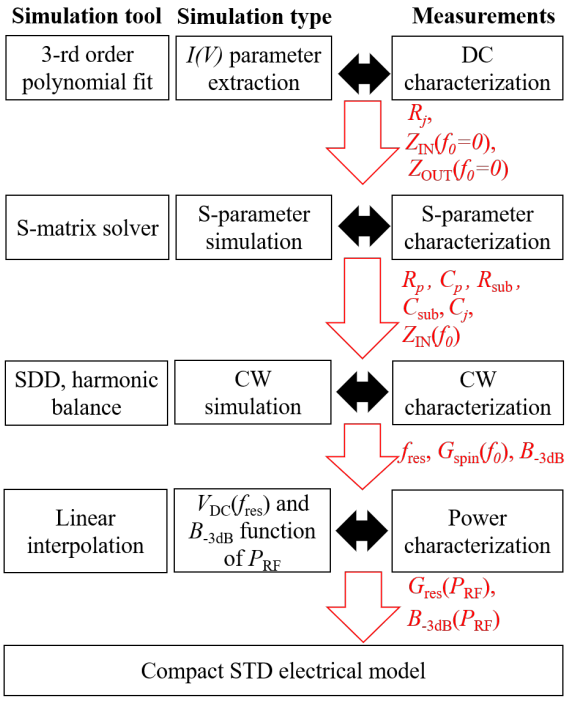

Fig. 13: Framework for extraction of STD electrical model parameters.

In Fig. 13, we summarize the methodology for parameter extraction of the STD model, with the different measurement steps and corresponding simulation tools. In Fig. 13, extracted

parameters are indicated in red color for each characterization/modeling step .

IV. Application of the Model to a Multiple STD-based RF detector

Thanks to their nano-sized footprint, multiple STD devices could be integrated in a complex RF detector architectures with the purpose of multiband RF detection or energy harvesting. This section proposes to model a multiple-based STD RF detector architecture using our compact electrical model for a standalone STD, with the objective of evaluating the RF-to-DC conversion efficiency of the detector.

A. Architecture at-hand: 2-STD based RF detector

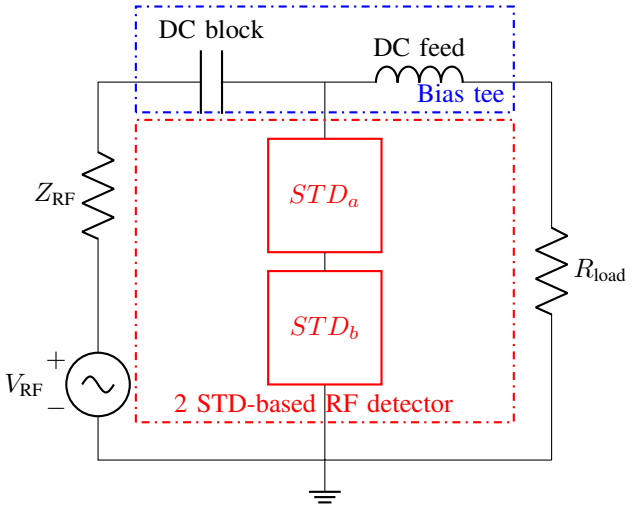

Fig. 14: CW characterization set-up for 2-STD based RF detector.

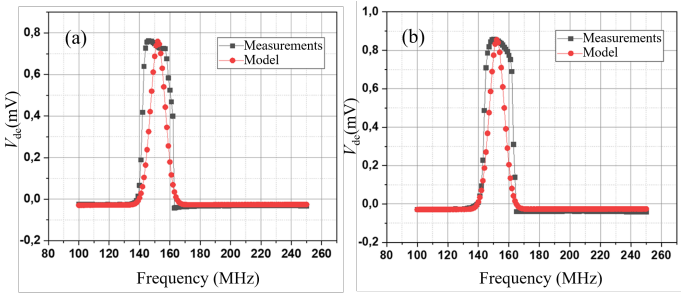

Fig. 15: CW characterization of (a) STD_a and (b) STD_b of the RF detector serial architecture.

The considered RF detector is composed of 2 STD devices connected in series, as seen in Fig. 14, with the use of wire-bonding. In the following sections, we propose to model this RF detector by connecting 2 STD equivalent circuits in series in order to evaluate the RF-to-DC conversion efficiency of the overall architecture. Simulation results from our electrical modeling will be compared to experimental measurements.

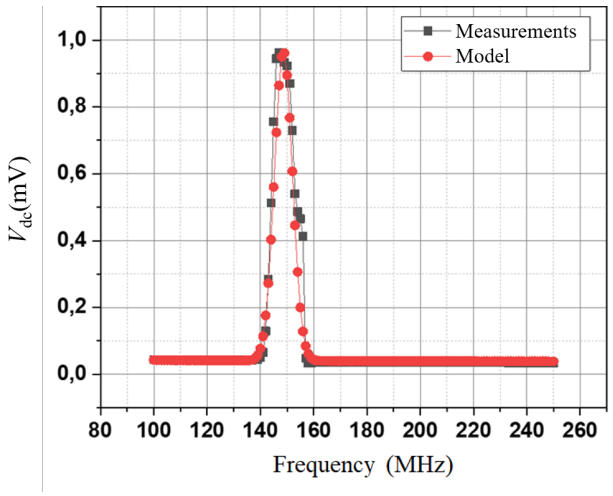

Fig. 16: CW characterization of STD_a and STD_b in series.

B. CW characterization vs model results

Fig. 15 (a) and (b) shows the measured output DC voltage, V_{dc}, for each STD device measured separately with CW characterization and considering an RF input power of -15 dBm. Simulation results for the output DC voltages for STD_a and STD_b, which are derived from our STD electrical model, are also reported on Fig. 15 (a) and (b), respectively (red plots). As it can be seen from Fig. 15, the maximum amplitudes for output DC voltages are correctly retrieved for both STDs. Fig. 16 shows the measured output DC voltage for the serial STD structure shown in Fig. 14. The model simulation perfectly matches with experimental measurement. Indeed, when 2 STDs, presenting the same input impedance, R_0 are placed in series, the input impedance of the serial structure is doubled, $Z_{IN} \approx 2R_0 = 68\ \Omega$ which slightly lowers the reflection coefficient, $|\Gamma(f_0)|^2$ from 0.036 to 0.023. However, since the input RF power feeding the serial structure is shared between both STDs, the overall generated DC voltage at the serial architecture output does not significantly overcome the DC voltage generated by a single STD (Fig. 15). This result, which is perfectly anticipated by our model, is particularly interesting in the purpose of considering multiple STD-based RF detector architectures. Our proposed STD electrical modeling paves the way for studying multiple STD based RF detectors, with the objective of defining a suitable architecture to improve the overall RF-to-DC conversion efficiency, when targeting single band or multi-band detection.

V. Conclusion

In this paper, we have proposed a compact electrical model for STD used as CW RF detector. It is based on i) the integration of the STD non-linear junction resistance through the evaluation of the STD $I(V)$ characteristics, ii) the STD input and output impedance modeling iii) the integration into the model of bandwidth and spin-torque gain dependency with RF input power. A detailed step-by-step methodology has been proposed to extract the model parameters using DC characterization, RF S-Parameter characterization, RF

CW characterization and finally RF power characterization. After parameter extraction, the model has been successfully validated: it provides accurate simulation results to estimate the STD output DC voltage considering an RF CW detection. To highlight the interest of using such an electrical model in a complex RF detector architecture, the RF-to-DC conversion efficiency of a multiple STD-based RF detector architecture has been evaluated. As a case study, a 2-STD based RF detector is modeled by connecting 2 STD electrical models in series. Simulation results show that RF-to-DC conversion efficiency is impacted by the modification of the impedance matching condition and by the input RF power sharing between the two series STD devices. As a consequence, the output DC voltage of the 2 STD-based RF detectors suffers from a RF-to-DC conversion efficiency penalty compared to a single STD-based RF detector. This RF-to-DC conversion efficiency penalty has been confirmed with experimental results. The proposed electrical model for STD and related framework to extract model parameters may constitute a good basis to derive suitable architectures for RF detectors using multiple STD devices, to address single band or multi-band detection.

A perspective of this work would be to go beyond the CW response of the STD, by integrating the STD band-pass limitation into an envelope simulation model. This would lead to the possibility of simulating the detection of digitally modulated RF carriers. As a second important perspective, it would be important to model the STD noise contributions, in order to provide an accurate estimation of the signal to noise ratio at STD output, with the final objective to estimate, using our compact model, the RF detector sensitivity.

VI. Acknowledgment

Authors would like to thank the International Iberian Nanotechnology Laboratory, Portugal, for providing STD devices. The authors acknowledge the support of the French Agence Nationale de la Recherche (ANR), under grant ANR-18-CE24-0012 (project SpinNet).

References

[1] A. Hirohata, K. Yamada, Y. Nakatani, *et al.*, "Review on spintronics: Principles and device applications," *Journal of Magnetism and Magnetic Materials*, vol. 509, p. 166 711, 2020.

[2] N. Leroux, A. Mizrahi, D. Marković, *et al.*, "Hardware realization of the multiply and accumulate operation on radio-frequency signals with magnetic tunnel junctions," *Neuromorphic Computing and Engineering*, vol. 1, no. 1, p. 011 001, 2021.

[3] D. Marković, N. Leroux, A. Mizrahi, *et al.*, "Detection of the microwave emission from a spin-torque oscillator by a spin diode," *Physical Review Applied*, vol. 13, no. 4, p. 044 050, 2020.

[4] T. Zeng, Y. Zhou, K. W. Lin, P. T. Lai, and P. W. T. Pong, "Spin-torque diode-based radio-frequency detector by utilizing tilted fixed-layer magnetization and in-plane free-layer magnetization," *IEEE Transactions on Magnetics*, vol. 51, no. 11, pp. 1–4, 2015.

[5] S. I. Kiselev, J. C. Sankey, I. N. Krivorotov, *et al.*, "Microwave oscillations of a nanomagnet driven by a spin-polarized current," *Nature*, vol. 425, pp. 380–383, 2003.

[6] S. Kaka, M. R. Pufall, W. H. Rippard, T. J. Silva, S. E. Russek, and J. A. Katine, "Mutual phase-locking of microwave spin torque nano-oscillators," *Nature*, vol. 437, no. 7057, pp. 389–392, Sep. 1, 2005.

[7] H. Maehara, H. Kubota, Y. Suzuki, *et al.*, "Large emission power over 2 μw with highiq/ifactor obtained from nanocontact magnetic-tunnel-junction-based spin torque oscillator," *Applied Physics Express*, vol. 6, no. 11, p. 113 005, Nov. 2013.

[8] W. Skowroński, M. Frankowski, J. Wrona, T. Stobiecki, P. Ogrodnik, and J. Barnaś, "Spin-torque diode radio-frequency detector with voltage tuned resonance," *Applied Physics Letters*, vol. 105, no. 7, p. 072 409, 2014.

[9] S. Hemour, Y. Zhao, C. H. P. Lorenz, *et al.*, "Towards low-power high-efficiency RF and microwave energy harvesting," *IEEE Transactions on Microwave Theory and Techniques*, vol. 62, no. 4, pp. 965–976, 2014.

[10] D. Marković, N. Leroux, A. Mizrahi, *et al.*, "Detection of the microwave emission from a spin-torque oscillator by a spin diode," *Phys. Rev. Applied*, vol. 13, p. 044 050, 4 Apr. 2020.

[11] R. Vauche, E. Muhr, O. Fourquin, *et al.*, "A 100 MHz PRF ir-uwb cmos transceiver with pulse shaping capabilities and peak voltage detector," *IEEE Transactions on Circuits and Systems I: Regular Papers*, vol. 64, no. 6, pp. 1612–1625, 2017.

[12] G. I. Evidente, S. Lorenzo Mindoro, A. Alvarez, *et al.*, "An ultra-low power direct active-rf detection wake-up receiver with noise-cancelling envelope detector in 65 nm cmos process," in *TENCON 2018 - 2018 IEEE Region 10 Conference*, 2018, pp. 0012–0015.

[13] Y. S. Gui, Y. Xiao, L. H. Bai, *et al.*, "High sensitivity microwave detection using a magnetic tunnel junction in the absence of an external applied magnetic field," *Applied Physics Letters*, vol. 106, no. 15, p. 152 403, 2015.

[14] S. Menshawy, A. S. Jenkins, K. J. Merazzo, *et al.*, "Spin transfer driven resonant expulsion of a magnetic vortex core for efficient RF detector," *AIP Advances*, vol. 7, no. 5, p. 056 608, 2017.

[15] M. Abbasi, B. Wang, S. Tamaru, H. Kubota, A. Fukushima, and D. S. Ricketts, "Accurate de-embedding and measurement of spin-torque oscillators," *IEEE Transactions on Magnetics*, vol. 53, no. 11, pp. 1–4, 2017.

[16] I. Bendjeddou, A. S. El Valli, A. Litvinenko, *et al.*, "Radio receivers based on spin-torque diodes as energy detectors," in *2021 19th IEEE International New Circuits and Systems Conference (NEWCAS)*, 2021, pp. 1–4.

[17] R. Sharma, R. Mishra, T. Ngo, *et al.*, "Electrically connected spin-torque oscillators array for 2.4GHz WiFi band transmission and energy harvesting," *Nature Communications*, vol. 12, no. 1, p. 2924, May 18, 2021.

[18] M. N. Baibich, J. M. Broto, A. Fert, *et al.*, "Giant magnetoresistance of (001) fe/(001) cr magnetic superlattices," *Physical review letters*, vol. 61, no. 21, p. 2472, 1988.

[19] G. Binasch, P. Grünberg, F. Saurenbach, and W. Zinn, "Enhanced magnetoresistance in layered magnetic structures with antiferromagnetic interlayer exchange," *Physical review B*, vol. 39, no. 7, p. 4828, 1989.

[20] A. A. Tulapurkar, Y. Suzuki, A. Fukushima, *et al.*, "Spin-torque diode effect in magnetic tunnel junctions," *Nature*, vol. 438, no. 7066, pp. 339–342, Nov. 1, 2005, ISSN: 1476-4687. [Online]. Available: https : / / doi . org / 10 . 1038 / nature04207.

[21] S. Miwa, S. Ishibashi, H. Tomita, *et al.*, "Highly sensitive nanoscale spin-torque diode," *Nature Materials*, vol. 13, no. 1, pp. 50–56, Jan. 1, 2014.

[22] V. S. Tiberkevich, A. N. Slavin, and J.-V. Kim, "Temperature dependence of nonlinear auto-oscillator linewidths: Application to spin-torque nano-oscillators," *Phys. Rev. B*, vol. 78, p. 092 401, 9 Sep. 2008.

[23] P. Li and L. Pileggi, "Efficient harmonic balance simulation using multi-level frequency decomposition," in *IEEE/ACM*

International Conference on Computer Aided Design, 2004. ICCAD-2004., 2004, pp. 677–682.

[24] P. A. Traverso, D. Mirri, G. Pasini, and F. Filicori, "A nonlinear dynamic S/H-ADC device model based on a modified volterra series: Identification procedure and commercial cad tool implementation," *Instrumentation and Measurement, IEEE Transactions on*, vol. 52, pp. 1129–1135, Sep. 2003.